Desalination and Water Treatment
www.deswater.com

doi: 10.5004/dwt.2017.21587

94 (2017) 254–262
October

Enhanced photocatalytic degradation of caffeine as a model pharmaceutical pollutant by Ag-ZnO-Al_2O_3 nanocomposite

Alaâeddine Elhalil[a], Rachid Elmoubarki[a], M'hamed Sadiq[a], Mohamed Abdennouri[a], Yassine Kadmi[b,c,d,e], Lidia Favier[f], Samir Qourzal[g], Noureddine Barka[a,*]

[a]*Laboratoire des Sciences des Matériaux, des Milieux et de la Modélisation (LS3M), FPK, Univ Hassan 1, B.P. 145, 25000 Khouribga, Morocco, Tel. +212678831928, email: elhalil.alaaeddine@gmail.com (A. Elhalil), Tel. +212661367831, email: elmoubarkirachid@gmail.com (R. Elmoubarki), Tel. +212666248196, email: sadiqmhamed@hotmail.com (M. Sadiq), Tel. +212667669039, email: abdennourimohamed@yahoo.fr (M. Abdennouri), Tel. +212 661 66 66 22, Fax +212 523 49 03 54, email: barkanoureddine@yahoo.fr (N. Barka)*
[b]*Université d'Artois, EA 7394, Institut Charles Viollette, Lens, F-62300, France, Tel.+33321603700, email: yassine.kadmi@gmail.com*
[c]*ISA Lille, EA 7394, Institut Charles Viollette, Lille, F-59000, France*
[d]*Ulco, EA 7394, Institut Charles Viollette, Boulogne sur Mer, F-62200, France*
[e]*Université de Lille, INRA, EA 7394, Institut Charles Viollette, Lille, F-59000, France*
[f]*Ecole Nationale Supérieure de Chimie de Rennes, CNRS, UMR 6226, 11 Allée de Beaulieu, CS 50837, 35708 Rennes Cedex 7, France, Tel.+33223238135, email: lidia.favier@ensc-rennes.fr (L. Favier)*
[g]*Equipe de Catalyse et Environnement, Faculté des Sciences, Université Ibn Zohr, B.P.8106 Cité Dakhla, Agadir, Morocco, email: (samir_qourzal@yahoo.fr)*

Received 23 June 2017; Accepted 22 October 2017

ABSTRACT

In this paper, an Ag-ZnO-Al_2O_3 nanocomposite with enhanced photocatalytic activity has been obtained by calcination of an Ag-loaded zinc/aluminum layered double hydroxide (LDH). First, LDH materials intercalated by carbonates ions (Zn-Al-CO_3) were synthesized by the co-precipitation method at a Zn/Al molar ratio of 3 and were calcined at different temperatures (300, 400, 500, 600, 800, and 1000°C). Thereafter, in order to increase photocatalytic activity, catalysts obtained at optimal temperature were doped by Ag noble metal with various amounts (1, 3, and 5 wt %) using a ceramic process. Samples were characterized by X-ray diffraction (XRD), Fourier transform infrared spectroscopy (FTIR), and scanning electron microscopy coupled to energy dispersive X-ray spectroscopy (SEM/EDX). The photocatalytic activity was evaluated for the degradation of caffeine as a model of pharmaceutical pollutant in aqueous solutions under UV irradiation. The effect of irradiation time, initial concentration of caffeine, catalyst dosage, solution pH, and reuse were investigated. The Ag-doped calcined LDH materials showed significantly higher photocatalytic activity compared with undoped and standard Degussa P-25 titanium dioxide. The photocatalytic degradation of caffeine was increased with an increase in the Ag-loaded amounts. The photocatalyst showed high stability after three regeneration cycles.

Keywords: Ag-ZnO-Al_2O_3; Mixed oxides; Photocatalytic activity; Caffeine; Pharmaceutical pollutants

1. Introduction

Caffeine (1,3,5-trimethylxanthine) is an alkaloid with widespread occurrence in a variety of foods and beverages such as coffee, tea, cola nuts, yerba mate, cocoa, and guarana [1,2]. Caffeine, which acts as stimulant for the heart, respiratory, and central nervous system and is a vasodilator and a diuretic [3], is a component of dietary supplements used for the improvement of athletic endurance and acceleration of weight loss [4]. These drugs carry a number of side effects,

*Corresponding author.

and an overdose of them can cause serious problems. However, caffeine can also cause advance mutation effects, cancer, heart disease, or complications in pregnant women [5]. Especially, caffeine is highly soluble in water [6]; further, persistent to biologic degradation in an environment, caffeine has been increasingly detected in influents and effluents of wastewater treatment plants, water supplies, and even drinking water [7].

Many different techniques have been applied for the removal of persistent molecules, e.g., adsorption [8], coagulation-flocculation [9], membrane filtration [10], biological treatments [11], Fenton process [12], and especially photocatalysis [13]. Among these techniques, photocatalysis is an effective and applicable method to degrade organic contaminants in wastewater. Heterogeneous photocatalysis has been proposed as a promising process to remove pollutants from air and water streams through the action of hydroxyl radicals (°OH) generated in the primary stages of these processes and possibility of pollutants oxidation to CO_2 and H_2O and mineral salts in the presence of semiconductors [14–16].

Recently, metal-oxide semiconductors and their derived composites with different morphologies and sizes have received considerable interest because of their good reaction stability and high photocatalytic activity for eliminating environmental pollution. Until now, different semiconductor materials, such as TiO_2 [17], WO_3 [18], ZnO [19], ZnS [20], Bi_2O_3 [21], CdS [22], etc., have been successfully applied in various photocatalytic systems. Among these materials, zinc oxide (ZnO) has remained one of the most widely used photocatalysts in recent years. The main advantages of this photocatalyst reside in its strong resistance to a wide variety of chemicals as well as to its high photosensitivity, nontoxic nature, and low cost [23]. However, a major limitation to achieving the high photocatalytic efficiency of a ZnO semiconductor is the rapid recombination of photo-excited electron/hole pairs [24,25]. To overcome these drawbacks, several methods have been designed by modifying the ZnO nanostructure. Recently, many nanocomposite-based ZnO, such as $ZnO/Ag/Ag_2WO_4$ [26], $Fe_3O_4/ZnO/NiWO_4$ [27], $Fe_3O_4/ZnO/CoWO_4$ [28], $ZnO/AgI/Ag_2CO_3$ [29], and $ZnO/Ag_3VO_4/AgI$, [30] have been prepared and applied in photocatalytic degradation of organic pollutants. The doping process by noble metals, such as Pt [31], Pd [32], Au [33], Ag [34], and Rh [32], is an effective strategy to enhanced photocatalytic activity of ZnO. From an economic point of view, Ag has been widely investigated compared with other noble metals.

A variety of preparation techniques have been reported for the synthesis of ZnO materials, such as sol–gel [35], hydrothermal synthesis method [36], chemical vapor deposition [37], photo-chemical reduction processes [38], co-precipitation methods [39], spray-pyrolysis methods [40], ultrasound-assisted methods [41], and microwave-assisted thermal decomposition [42]. By using layered double hydroxides (LDHs) as a precursor for the preparation of ZnO, it is possible to obtain fine dispersion of active components on the surface of a semiconductor and, as a consequence, the formation of an intimate contact at atomic level between the generated semiconductor phases. Moreover, Al in the structure has more advantages over a ZnO photocatalyst owing to its high photocatalytic activity, morphology, particle size, low cost, and good stability [43–45].

In this research, ZnO-Al_2O_3 mixed oxides have been prepared by calcination of a Zn/Al-layered double hydroxide. For improving the photocatalytic performance, the samples were doped by different amounts of Ag noble metal (1, 3, and 5 wt %) using a ceramic process. The catalysts were characterized by several physico-chemical techniques (XRD, FTIR, and SEM/EDX). The photocatalytic activity of prepared photocatalysts was evaluated for the degradation of caffeine as a model of pharmaceutical pollutant under UV irradiation. The effect of Ag doping concentration on the photocatalytic activity was evaluated in detail.

2. Experimental

2.1. Reagents

The starting chemicals – zinc nitrate ($Zn(NO_3)_2{\cdot}6H_2O$), aluminum nitrate ($Al(NO_3)_3{\cdot}9H_2O$), silver nitrate ($AgNO_3$), sodium carbonate (Na_2CO_3), sodium hydroxide (NaOH) and hydrochloric acid, 37% (HCl) and Degussa P-25 titanium dioxide – have been acquired from Sigma-Aldrich (Germany). Caffeine ($C_8H_{10}N_4O_2$) was a product of Sigma-Aldrich (China). All the used chemicals were of analytical grade and employed without further purification. Bi-distilled water was used as the solvent throughout this study.

2.2. Characterization

The XRD measurements were performed at room temperature on a D2 PHASER diffractometer, with Bragg–Brentano geometry, using a CuK_α target (λ = 1.5406 Å) operating at 30 KV and 10 mA. Fourier transform infrared (FTIR) spectra in KBr pellets were collected on a Perkin Elmer (FTIR-2000) spectrophotometer, in the range of 4000–400 cm^{-1}. The external surface of a sample was analyzed by scanning electron microscopy coupled to the energy-dispersive X-ray spectroscopy (SEM/EDX) using a FEI Quanta 200 model.

2.3. Catalysts preparation

2.3.1. Synthesis of LDH precursor and calcination

A Zn-Al-layered double hydroxide material intercalated with carbonate anions was prepared by co-precipitation method from metal salts. The molar cationic ratio r = Zn/Al was fixed to 3. A mixture solution of $Zn(NO_3)_2{\cdot}6H_2O$ and $Al(NO_3)_3{\cdot}9H_2O$, with a total concentration of metal ions of 2 mol/L and Na_2CO_3 (1 mol/L), was added dropwise in a backer containing 50 mL of bi-distilled water. The pH of the mixture was adjusted and kept constant at 8.5 ± 0.2 during the synthesis by adding suitable amounts of NaOH (2 M) solution. The formed gel was kept under constant magnetic stirring for 4 h. The final products were recuperated by filtration, washed several times with bi-distilled water until pH = 7, and dried at 100°C for 24 h. The mixed-oxide photocatalysts were prepared by calcination of a LDH precursor at different temperatures (300, 400, 500, 600, 800, and 1000°C) for 6 h in a muffle furnace.

2.3.2. Solid-state impregnation

The desired amount of LDH precursor and $AgNO_3$ were manually ground in an agate mortar for 30 min. After that, the homogeneously mixed powder was transferred into a crucible and calcined in air at 500°C for 6 h in a muffle furnace. The entire process is free of solvents. The obtained samples were denoted as x%-Ag-LDH, where x% represents the weight percentage of Ag in the mixture (1, 3, and 5 wt %).

2.4. Photocatalytic experiments

Photocatalytic experiments were carried out in a cylindrical quartz photoreactor with a capacity of 2 L irradiated by a UV mercury lamp (400 W) and placed in the center of the reactor. The temperature was maintained at 25 ± 2°C by connecting the reactor to circulating water to prevent the lamp from overheating. Experiments were done using 0.3 g/L of each photocatalyst with an initial concentration of 20 mg/L caffeine. Prior to the catalytic experiments, the aqueous solution of the caffeine and the catalyst was stirred for 1 h in order to attain adsorption equilibrium in the dark. At different time intervals, 3 mL of the solution were extracted and filtered. The concentration of caffeine was monitored by measuring the absorbance at 273 nm [46], using a double-beam scanning spectrophotometer (Shimadzu spectrophotometer, model biochrom). The blank reaction was carried out following the same procedure without adding a catalyst.

3. Results and discussion

3.1. Catalyst characterization

3.1.1. X-ray diffraction study

XRD patterns of LDH precursors before and after calcination are shown in Fig. 1(a). The figure shows reticular planes (003), (006), (012), (015), (018), (110), and (113) typical of the LDH structure. No impurities from any residual $Zn(OH)_2$ or $Al_2(OH)_3$ were observed. Remarkable changes are observed after calcination. The well-defined diffraction peaks of the parent samples were replaced by broad peaks, thus indicating a poor long-range ordered phase. These broad peaks suggest a nanocrystalline material with small nanoparticles or even an amorphous phase. The lamellar structure collapsed, and new peaks corresponding to ZnO oxide and $ZnAl_2O_4$ spinel phases started to appear with the rise in temperature [47]. The characteristic XRD peaks of ZnO oxide started to first appear at 300°C, indicated by the peaks at 2θ = 31.8°, 34.5°, 36.3°, 47.6°, 56.6°, 62.9°, 66.4°, 68°, and 69.1°. These peaks correspond to the reflections from (100), (002), (101), (102), (110), (103), (200), (112), and (201) planes, respectively; this is also confirmed by the JCPDS data (Card No. 36-1451) [48]. Total dehydroxylation was observed at 500°C and resulted in the transformation of LDH structure to corresponding metal-oxides ZnO and Al_2O_3. At calcination temperatures of 600°C and above, $ZnAl_2O_4$ spinel phase appears, as observed by diffraction peaks at 2θ = 31.2°, 36.75°, 44.7°, 49.1°, 55.6°, 59.3°, and 65.3°. These peaks correspond to the reflections from (220), (311), (400), (331), (422), (511), and (440) planes, respectively (JCPDS Card No. 05-0669) [49]. The relative intensity of $ZnAl_2O_4$ peaks increased as the calcination temperature increased.

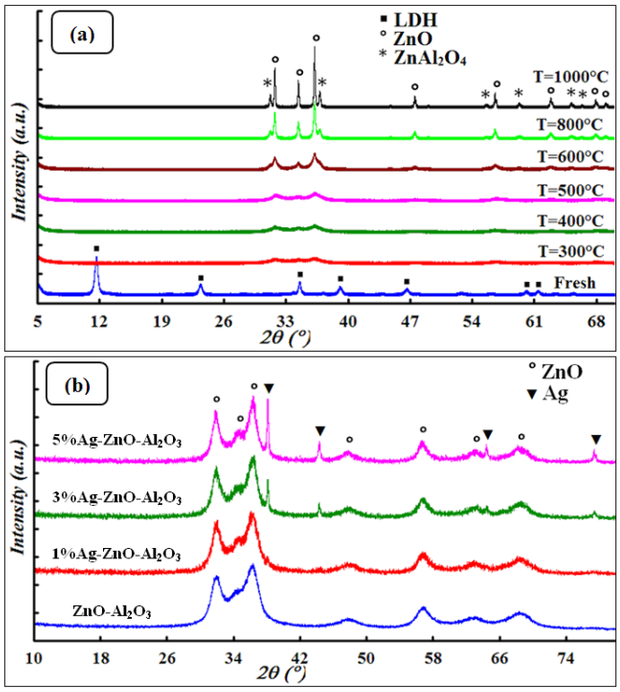

Fig. 1. XRD patterns of the fresh and calcined LDH (a), undoped and Ag doped (b).

For Ag-doped LDH samples [Fig. 1(b)], four additional peaks at 38.24°, 44.42°, 64.44°, and 77.40° were observed. These peaks can be assigned to (111), (200), (220), and (311) reflections of the face centered cubic metallic Ag nanoparticles (JCPDS card No. 04-0783) [50]. The crystallinity of Ag nanoparticles was much sharper and increases with increasing Ag content. No peaks from other phases were detected, indicating high purity of the products.

3.1.2. Fourier transform infrared spectra

Fig. 2 represents the FTIR spectra of the fresh LDH precursor, undoped and Ag-doped LDH calcined at 500°C. The spectrum of the fresh LDH precursor shows a broad band between 3600 and 3200 cm^{-1}, which is attributed to the stretching vibration of the OH groups of physically adsorbed and interlamellar water molecules. The band at 1617 cm^{-1} was due to O–H bending vibration of the interlayer water molecules [51]. The band at 1364 cm^{-1} is assigned to the stretching vibration of the CO_3^{2-} groups in the LDH interlayer [52]. This band rapidly disappears after calcination, which is attributed to the thermal decomposition of carbonate ions. Bands around 700–400 cm^{-1} could be related to the lattice vibration modes such as the translation vibrations by M-O (590 and 670 cm^{-1}) and O-M-O (430 cm^{-1}) [53].

3.1.3. SEM/EDX observation

Fig. 3 displays the surface morphology and crystallite structure of undoped and 5% Ag-doped ZnO-Al_2O_3. The

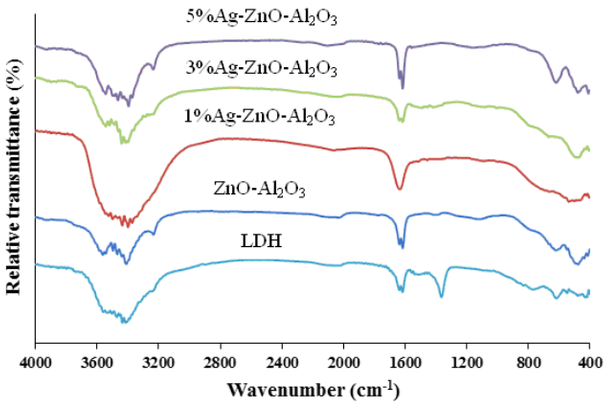

Fig. 2. FTIR spectra of fresh LDH precursor, undoped and Ag doped calcined LDH.

images indicate an obvious difference in morphology between undoped and Ag-doped ZnO-Al_2O_3 composite. The particle size of the undoped and doped composite varied from 4 to 10 nm. After Ag doping, Ag particles were homogeneously and highly dispersed on the surface of ZnO-Al_2O_3 composite. Energy dispersive X-ray spectrum (EDX) of undoped and Ag-doped nanocomposite is shown in Figs. 3b–d. The results confirm the presence of Zn, Al, and O in the undoped sample. For Ag-ZnO-Al_2O_3 composite, the spectrum shows peaks corresponding to Ag, along with the other constituent elements (Zn, Al, and O).

4. Photocatalytic study

4.1. Effect of calcination temperature

Fig. 4 shows the comparison of photocatalytic activity of LDH calcined at different temperatures and compared with a standard Degussa P-25 photocatalyst. Before UV-light irradiation, each suspension of photocatalyst/caffeine solutions was continuously stirred in the dark for 60 min to reach an adsorption–desorption equilibrium. In the same operating conditions for the photocatalytic degradation, the photolytic degradation without photocatalysts was studied. After 180 min of irradiation, a low diminution of the concentration of caffeine was observed. According to this result, we can neglect the interference of the photolytic degradation with the photocatalytic degradation.

Fig. 4 shows that the calcination temperature has a great influence on the photocatalytic activity. With increasing the calcination temperature to 300 and 400°C, the photocatalytic activity obviously increases owing to the beginning of formation of ZnO oxide. At 500°C, the sample shows the highest photocatalytic activity. The photocatalyst calcined at 500°C exhibited good photocatalytic activity as compared with the other calcination temperature. This can be usually interpreted by the crystallization of ZnO [54], which is an important factor influencing the photocatalytic activity. Beyond the 600°C, the photocatalytic performance starts to decrease. This result can be

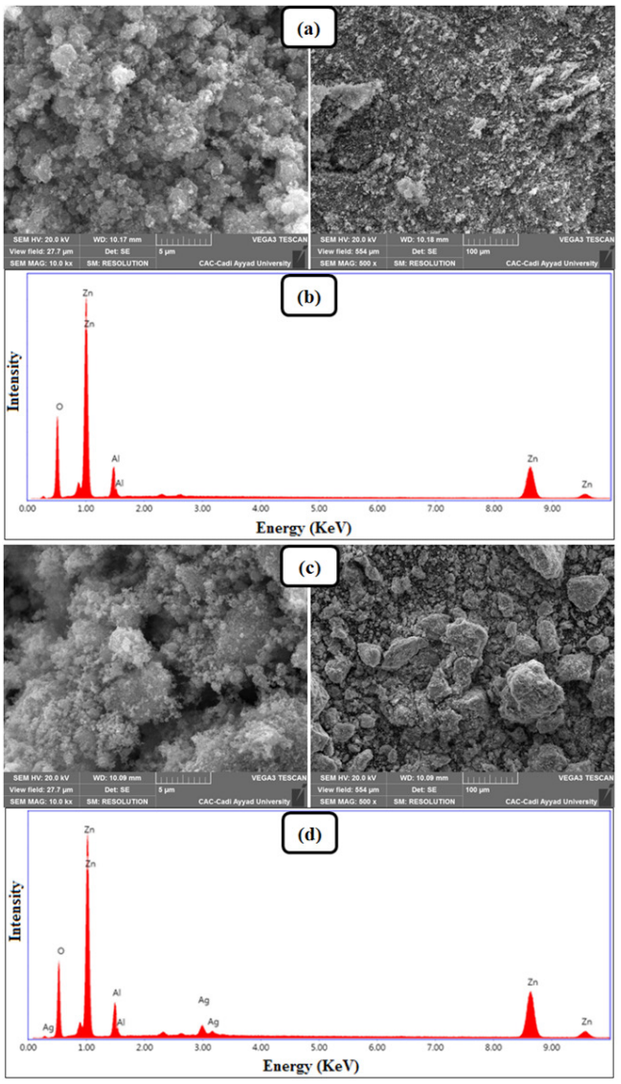

Fig. 3. SEM-EDX images of undoped (a, b) and Ag doped composite (c, d).

attributed to low adsorption observed in the first 60 min in the dark. Thus, from T = 600°C, the ZnO oxide in the calcined catalysts starts to be transformed into $ZnAl_2O_4$, which is *photocatalytically inactive*. These results suggest that adsorption performance and amount and degree of crystallization of active component (ZnO) were the essential factors directly influencing the photocatalytic degradation of caffeine.

4.2. Effect of Ag doping

For increasing the photocatalytic activity of the best catalyst calcined at 500°C, the material was doped by Ag noble metal with various amounts (1, 3, and 5 wt %) using a ceramic process. The results illustrated in Fig. 5 reveal that the doped catalysts displayed excellent photocatalytic performance compared with undoped catalysts. It can be seen

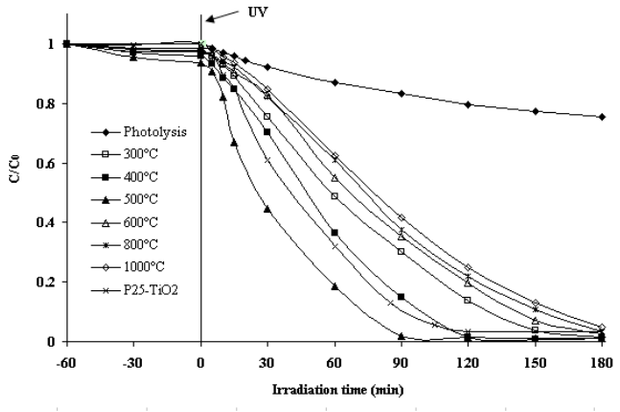

Fig. 4. Effect of calcination temperature on the photocatalytic degradation of caffeine compared to standard Degussa P-25 TiO_2.

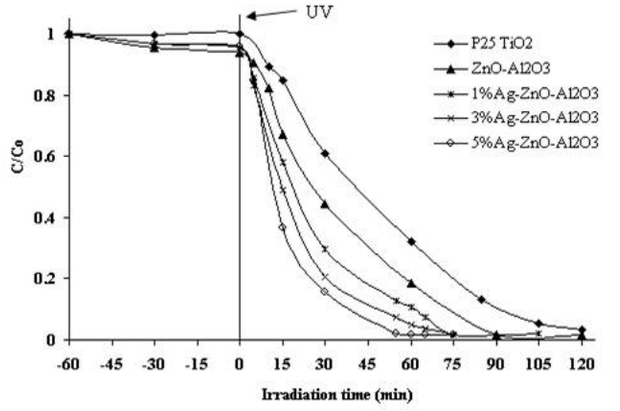

Fig. 5. Photocatalytic degradation of caffeine in the presence of undoped and Ag doped calcined LDH.

from the figure that the degradation rate slightly increased with the increase of Ag loading. The experimental results indicated that a high amount of Ag (5%) shows the highest catalytic activity. After 55 min of irradiation, the complete degradation of caffeine was done.

The figure also indicates that the adsorption rate decreased after Ag doping. Therefore, the increase in photocatalytic activity of catalysts is mainly due to the synergistic effects between Ag noble metal and ZnO oxide. The relation between the amount of Ag in the catalyst and the photocatalytic degradation rate can be explained by the fact that Ag acts as an electron trap. The electrons generated on the ZnO surface by UV light illumination quickly move to the Ag particle to facilitate the effective separation of the photogenerated electron and holes, resulting in the significant enhancement of photocatalytic activity [55]. Ag plays a positive role as electron acceptor, more acceptor centers are provided with increasing Ag doping; therefore, the degradation rate for caffeine increases with the increase of Ag content.

4.3. Effect of photocatalyst dose

In order to avoid an excess catalyst and ensure total absorption of efficient photons, a series of experiments was carried out to assess the optimum catalyst loading by varying the amount of best photocatalyst (5% Ag-ZnO-Al_2O_3) from 0.1 to 1.5 g/L. Experiments were done in a 20 mg/L caffeine aqueous solution at a 7.5 pH solution. After 55 min of UV irradiation, the photocatalytic degradation efficiency (%) was evaluated. Results given in Fig. 6 show that the increase of catalyst dose from 0.1 to 0.3 g/L resulted in an increase in the photocatalytic degradation efficiency from 83.52 to 99.3%. Beyond this dose, a slight decrease in the degradation efficiency with the rise of the catalyst dose was observed. This can be explained by the fact that an excess photocatalyst dose resulted in unfavorable light scattering and reduction of light penetration into the solution. The same comportment was observed by Qourzal et al. [56]. From a practical viewpoint, the optimum dosage of 0.3 g/L was chosen in further experiments.

4.4. Effect of initial solution pH

The effect of solution pH on photocatalytic oxidation of caffeine in the presence of 5% Ag-ZnO-Al_2O_3 was studied at pH of 3.5, 7.5, 9.5, and 11. Fig. 7 shows that the pH solution significantly affected the degradation rate of caffeine. The photocatalytic activity was enhanced at a pH of 9.5 and was dramatically decreased at a pH of 3.5. Generally, the pH solution significantly affects, at the same time, the surface charge of the photocatalyst. The pH_{pzc} of 5% Ag-ZnO-Al_2O_3 catalyst was found to be 9.38. Therefore, at pH > 9.38, the surface acquired a negative charge, favoring the adsorption of cationic molecules. While at pH < 9.38, the surface of the catalyst acquired a negative charge, favoring the adsorption of anionic molecules. The pKa of caffeine molecule is 10.4, which means that the molecule is fully protonated at pH < 10.4.

Because the structure of caffeine was the same in the region of the studied pH, the observed behavior could be only due to the modification of the proprieties of the photocatalysts. The observed trend of the photocatalytic activity observed at pH of 9.5 could be due to the enhanced adsorption of caffeine on the photocatalyst favored at pH between 9.38 and 10.4 (Fig. 8) and more efficient formation of hydroxyl radicals [57]. If the pH rises above pKa = 10.4, then caffeine will be deprotonated and exist in a stable form as a starting molecule. Thus, the caffeine molecule is neutral. Therefore, at pH = 11 the adsorption process decreases with a slight decrease in the photocatalytic activity of the catalyst. In an acidic medium (pH = 3.5), the decrease of degradation rate could be attributed to many phenomena simultaneously intervening: a) nonfavorable adsorption; b) the dissolution of the photocatalysts; and c) the photodecomposition and dissolution of ZnO according to the following equations [58,59]:

$$\text{Dissolution: } ZnO + 2H^+ \rightarrow Zn^{2+}_{(aq)} + H_2O \quad (1)$$

$$\text{Photodecomposition: } ZnO + 2h^+_{VB} \rightarrow Zn^{2+}_{(aq)} + O^* \quad (2)$$

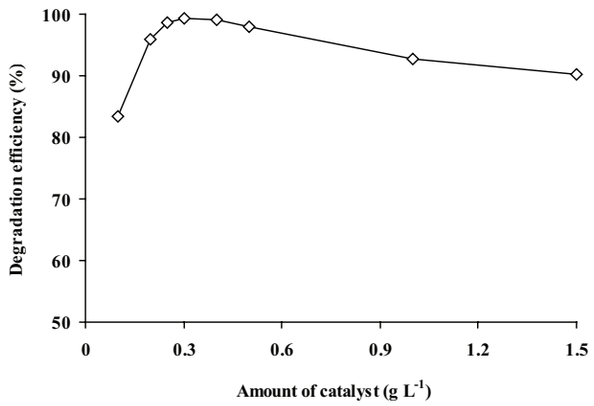

Fig. 6. Effect of catalyst dose on the photocatalytic degradation of caffeine.

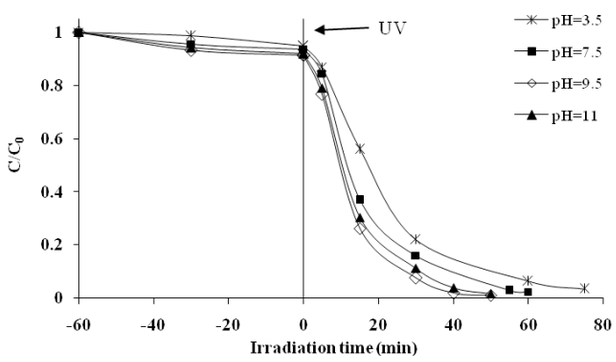

Fig. 7. Effect of initial solution pH of the photocatalytic degradation of caffeine.

4.5. Effect of initial concentration of caffeine

The effect of initial concentration of caffeine (5–30 mg/L) on its photocatalytic degradation was studied at the initial solution pH of 7.5 and the optimum catalyst dose of 0.3 g/L. From Fig. 9, it is evident that the photocatalytic degradation depends on the initial concentration of caffeine. Because the lifetime of hydroxyl radicals is short (only a few nanoseconds), they can only react at or remain near the location where they are formed. A high caffeine concentration logically enhances the probability of collision with oxidizing species, leading to an increase in the degradation rate.

According to numerous works [60,61], the influence of the initial concentration of the solute on the photocatalytic degradation rate of most organic compounds is described by pseudo-first order kinetics:

$$r = -\frac{dC}{dt} = k_{ap}C \tag{3}$$

Integration of Equation (3) will lead to the expected relation:

$$\ln\left(\frac{C_o}{C}\right) = k_{ap}\,t \tag{4}$$

where k_{ap} is the apparent reaction rate constant (min^{-1}), t is the irradiation time, C_0 is the initial concentration of caffeine, and C is the concentration of caffeine at a reaction time t.

The plot of ln (C_0/C) versus t with a different initial concentration of caffeine is shown in Fig. 10. The figure shows that the photocatalytic degradation fully follows the pseudo first-order kinetic in the case of initial concentrations of 5, 10, and 15 mg/L. However, for concentrations greater than 15 mg/L, the photocatalytic degradation takes place

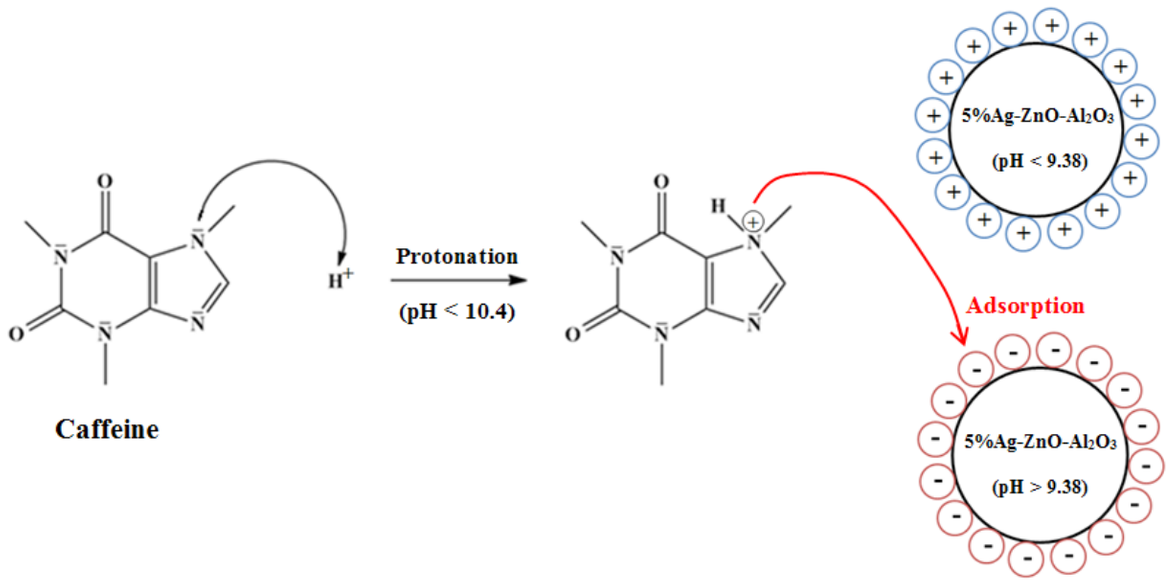

Fig. 8. Schematic illustration of adsorption process at different pH (pH < pH_{pzc} and pH > pH_{pzc}).

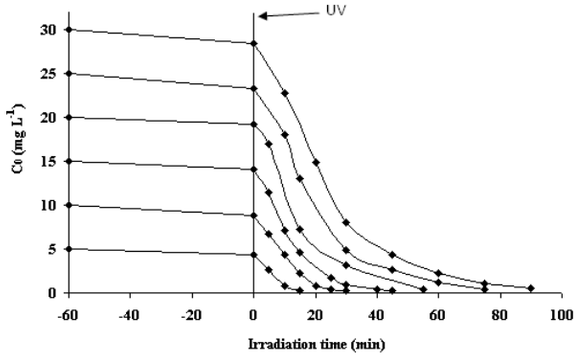

Fig. 9. Photocatalytic degradation of caffeine at different initial concentrations.

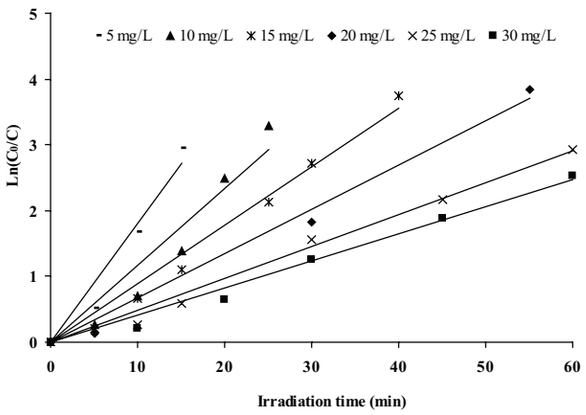

Fig. 10. Plot of ln (C_0/C) versus t with different initial concentrations of caffeine.

in two stages, the first stage of the process follows a pseudo-first-order kinetic with respect to caffeine concentrations and a second slower stage until the end of the process of the photocatalytic degradation. The time length of the first stage decreases with increasing the initial caffeine concentration. This result can be explained by the competitive adsorption/degradation behavior between caffeine molecules and its degradation intermediates, which could be more significant with a high concentration in the solution.

The effect of initial caffeine concentration on the initial rate of degradation is shown in Fig. 11. The figure indicates that the initial rate of degradation increases with increasing the initial concentration of caffeine until 20 mg/L; then, it starts to decrease with the rise in concentration in the solution. This can be explained by the fact that, with an increase in the number of caffeine molecules, the path length of photons entering the solution decreases and fewer photons reach the catalyst surface; thus, the generation of hydroxyl and superoxide radicals gets reduced. The optimum concentration of caffeine was found to be 20 mg/L.

4.6. Efficiency of regenerated photocatalyst

Generally, recycling of the photocatalyst is crucially important for industrial applications. In order to determine

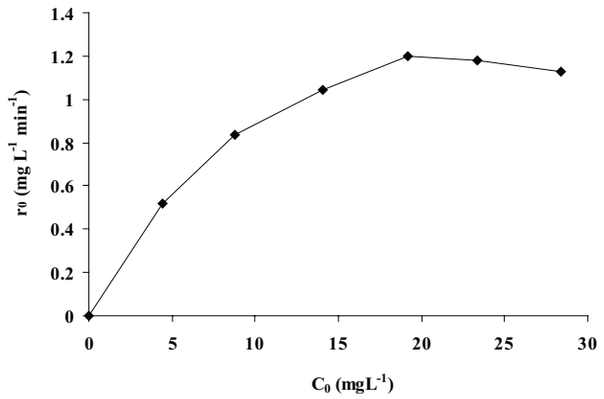

Fig. 11. Effect of initial concentration of caffeine on its initial rate of degradation.

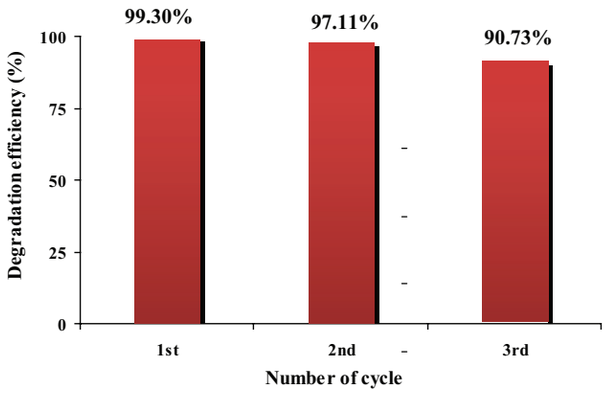

Fig. 12. Photocatalytic degradation of caffeine over three cycles of regeneration of 5% Ag-ZnO-Al_2O_3 photocatalyst.

the recyclability of the best catalyst, we carried out a cycle of experiments under identical conditions. The suspension was recovered by centrifugation, washed with distilled water to remove the residual caffeine, and dried at 100°C before another catalytic test. As illustrated in Fig. 12, the photocatalytic activity of the prepared photocatalyst still maintains at a high level even after cycling three times. There was no significant catalyst deactivation after three cycling runs, confirming that 5% Ag-ZnO-Al_2O_3 photocatalysts are highly efficient and very stable.

5. Conclusion

In summary, Ag-ZnO-Al_2O_3 photocatalysts were prepared by a facile single step deposition of Ag noble metal onto Zn/Al LDH precursor at different contents. The prepared catalysts were characterized using several techniques such as XRD, FTIR and SEM/EDX. The photocatalytic activity of the catalysts was evaluated for the degradation of caffeine as a model of pharmaceutical pollutant in aqueous solution under UV irradiation. The x%Ag-ZnO-Al_2O_3 photocatalyst exhibited an excellent photocatalytic activity toward the degradation of caffeine, in comparison to

undoped ZnO-Al_2O_3 and commercial P-25 photocatalysts. The maximum photocatalytic degradation (99.3%) of the caffeine was achieved by 5%Ag-ZnO-Al_2O_3 sample after 55 min of irradiation. The LDH precursor with a facile preparation and low cost products helps to obtain the catalysts with good stability, best crystallinity and good dispersion properties. The enhanced photocatalytic activity was mainly attributed to the interfacial heterostructure in the 5%Ag-ZnO-Al_2O_3 catalyst. This study could provide new route for the fabrication of high performance photocatalysts based on Ag-ZnO-Al_2O_3 and facilitate their application in the environmental remediation issues.

References

[1] J.L. Blauch, S.M. Tarka, HPLC determination of caffeine and theobromine in coffee, tea, and instant hot cocoa mixes, J. Food Sci., 48 (1983) 745–747.

[2] H. Sereshti, S. Samadi, A rapid and simple determination of caffeine in teas, coffees and eight beverages, Food Chem., 158 (2014) 8–13.

[3] X. Jun, Caffeine extraction from green tea leaves assisted by high pressure processing, J. Food Eng., 94 (2009) 105–109.

[4] O. Cauli, M. Morelli, Caffeine and the dopaminergic system, Behav. Pharmacol., 16 (2005) 63–77.

[5] J.Y. Sun, K.J. Huang, S.Y. Wei, Z.W. Wu, F.P. Ren, A graphene-based electrochemical sensor for sensitive determination of caffeine, Colloids Surf. B: Biointerfaces., 84 (2011) 421–426.

[6] P. Sriamornsak, R.A. Kennedy, Effect of drug solubility on release behavior of calcium polysaccharide gel-coated pellets, Eur. J. Pharm. Sci., 32 (2007) 231–239.

[7] F. Sodré, M. Locatelli, W. Jardim, Occurrence of emerging contaminants in brazilian drinking waters: a sewage-to-tap issue, Water Air Soil Pollut., 206 (2010) 57–67.

[8] C. Wang, Y. Le, B. Cheng, Fabrication of porous ZrO_2 hollow sphere and its adsorption performance to Congo red in water, Ceram. Int., 40 (2014) 10847–10856.

[9] T.K.F.S. Freitas, V.M. Oliveira, M.T.F. De Souza, H.C.L. Geraldino, V.C. Almeida, S.L. Fávaro, J.C. Garcia, Optimization of coagulation-flocculation process for treatment of industrial textile wastewater using okra (A. esculentus) mucilage as natural coagulant, Ind. Crops Prod., 76 (2015) 538–544.

[10] M. Taheran, S.K. Brar, M. Verma, R.Y. Surampalli, T.C. Zhang, R.J. Valero, Membrane processes for removal of pharmaceutically active compounds (PhACs) from water and wastewaters, Sci. Total Environ., 547 (2016) 60–77.

[11] B. Bonakdarpour, I. Vyrides, D.C. Stuckey, Comparison of the performance of one stage and two stage sequential anaerobice aerobic biological processes for the treatment of reactive-azo-dye-containing synthetic wastewaters, Int. Biodeterior. Biodegrad., 65 (2011) 591–599.

[12] A. Elhalil, H. Tounsadi, R. Elmoubarki, F.Z. Mahjoubi, M. Farnane, M. Sadiq, M. Abdennouri, S. Qourzal, N. Barka, Factorial experimental design for the optimization of catalytic degradation of malachite green dye in aqueous solution by Fenton process, Water Resour. Ind., 15 (2016) 41–48.

[13] M. Abdennouri, A. Elhalil, M. Farnane, H. Tounsadi, F.Z. Mahjoubi, R. Elmoubarki, M. Sadiq, L. Khamar, A. Galadi, M. Baâlala, M. Bensitel, Y. El hafiane, A. Smith, N. Barka, Photocatalytic degradation of 2,4-D and 2,4-DP herbicides on Pt/TiO nanoparticles, J. Saudi Chem. Soc., 19 (2015) 485–493.

[14] X.Q. Deng, X. Zhu, Z.G. Sun, X.S. Li, J.L. Liu, C. Shi, A.M. Zhu, Exceptional activity for photocatalytic mineralization of formaldehyde over amorphous titania nanofilms, Chem. Eng. J., 306 (2016) 1001–1009.

[15] C. Diaz-Uribe, W. Vallejo, W. Ramos, Methylene blue photocatalytic mineralization under visible irradiation on TiO_2 thin films doped with chromium, Appl. Surf. Sci., 319 (2014) 121–127.

[16] G. Liao, D. Zhu, J. Zheng, J. Yin, B. Lan, L. Li, Efficient mineralization of bisphenol A by photocatalytic ozonation with TiO_2–graphene hybrid, J. Taiwan Inst. Chem. Eng., 67 (2016) 300–305.

[17] H.L. Shen, H.H. Hu, D.Y. Liang, H.L. Meng, P.G. Li, W.H. Tang, C. Cui, Effect of calcination temperature on the microstructure, crystallinity and photocatalytic activity of TiO_2 hollow spheres, J. Alloys Compd., 542 (2012) 32–36.

[18] H. Zhang, J. Yang, D. Li, W. Guo, Q. Qin, L. Zhu, W. Zheng, Template-free facile preparation of monoclinic WO3 nanoplates and their high photocatalytic activities, Appl. Surf. Sci., 305 (2014) 274–280.

[19] R. Khan, M.S. Hassan, L.W. Jang, J.H. Yun, H.K. Ahn, M.S. Khil, I.H. Lee, Low-temperature synthesis of ZnO quantum dots for photocatalytic degradation of methyl orange dye under UV irradiation, Ceram. Int., 40 (2014) 14827–14831.

[20] Q. Ma, Y. Wang, J. Kong, H. Jia, Tunable synthesis, characterization and photocatalytic properties of various ZnS nanostructures, Ceram. Int., 42 (2016) 2854–2860.

[21] D. Sánchez-Martínez, I. Juárez-Ramírez, L.M. Torres-Martínez, I. De León-Abarte, Photocatalytic properties of Bi_2O_3 powders obtained by an ultrasound-assisted precipitation method, Ceram. Int., 42 (2016) 2013–2020.

[22] Z. Yu, B. Yin, F. Qu, X. Wu, Synthesis of self-assembled CdS nanospheres and their photocatalytic activities by photodegradation of organic dye molecules, Chem. Eng. J., 258 (2014) 203–209.

[23] C. Tian, Q. Zhang, A. Wu, M. Jiang, Z. Liang, B. Jiang, H. Fu, Cost-effective large-scale synthesis of ZnO photocatalyst with excellent performance for dye photodegradation, Chem. Commun., 48 (2012) 2858–2860.

[24] K.M. Lee, C.W. Lai, K.S. Ngai, J.C. Juan, Recent developments of zinc oxide based photocatalyst in water treatment technology: A review, Water Res., 88 (2016) 428–448.

[25] H. Osman, Z. Su, X. Ma, S. Liu, X. Liu, D. Abduwayit, Synthesis of ZnO/C nanocomposites with enhanced visible light photocatalytic activity, Ceram. Int., 42 (2016) 10237–10241.

[26] M. Pirhashemi, A. Habibi-Yangjeh, Ultrasonic-assisted preparation of plasmonic ZnO/Ag/Ag_2WO_4 nanocomposites with high visible-light photocatalytic performance for degradation of organic pollutants, J. Colloid Interface Sci., 491 (2017) 216–229.

[27] A. Habibi-Yangjeh, M. Shekofteh-Gohari, Novel magnetic Fe_3O_4/ZnO/$NiWO_4$ nanocomposites: Enhanced visible-light photocatalytic performance through p-n heterojunctions, Sep. Purif. Technol., 184 (2017) 334–346.

[28] M. Shekofteh-Gohari, A. Habibi-Yangjeh, Fe_3O_4/ZnO/$CoWO_4$ nanocomposites: Novel magnetically separable visible light-driven photocatalysts with enhanced activity in degradation of different dye pollutants, Ceram. Int., 43 (2017) 3063–3071.

[29] B. Golzad-Nonakaran, A. Habibi-Yangjeh, Ternary ZnO/AgI/Ag_2CO_3 nanocomposites: Novel visible-light-driven photocatalysts with excellent activity in degradation of different water pollutants, Mater. Chem. Phys., 184 (2016) 210–221.

[30] B. Golzad-Nonakaran, A. Habibi-Yangjeh, Photosensitization of ZnO with Ag_3VO_4 and AgI nanoparticles: Novel ternary visible-light-driven photocatalysts with highly enhanced activity, Adv. Powder Technol., 27 (2016) 1427–1437.

[31] L. Muñoz-Fernandez, A. Sierra-Fernandez, O. Miloševiæ, M.E. Rabanal, Solvothermal synthesis of Ag/ZnO and Pt/ZnO nanocomposites and comparison of their photocatalytic behaviors on dyes degradation, Adv. Powder Technol., 27 (2016) 983–993.

[32] C. Yu, K. Yang, W. Zhou, Q. Fan, L. Wie, J.C. Yu, Preparation, characterization and photocatalytic performance of noble metals (Ag, Pd, Pt, Rh) deposited on sponge-like ZnO microcuboids, J. Phys. Chem. Solids., 74 (2013) 1714–1720.

[33] M.M. Ismail, W.Q. Cao, M.D. Humadi, Synthesis and optical properties of Au/ZnO core–shell nanorods and their photocatalytic activities, Optik., 127 (2016) 4307–4311.

[34] O. Bechambi, M. Chalbi, W. Najjar, S. Sayadi, Photocatalytic activity of ZnO doped with Ag on the degradation of endocrine disrupting under UV irradiation and the investigation of its antibacterial activity, Appl. Surf. Sci., 347 (2015) 414–420.

[35] B. Astinchap, R. Moradian, M.N. Tekyeh, Investigating the optical properties of synthesized ZnO nanostructures by sol-gel: The role of zinc precursors and annealing time, Optik., 127 (2016) 9871–9877.
[36] B. Liu, H.C. Zeng, Hydrothermal synthesis of ZnO nanorods in the diameter regime of 50 nm, J. Am. Chem. Soc., 125 (2003) 4430–4431.
[37] Y. Liu, M. Liu, Ordered ZnO nanorods synthesized by combustion chemical vapor deposition, J. Nanosci. Nanotechnol., 7 (2007) 4529–4533.
[38] G. Oster, M. Yamamoto, Zinc oxide sensitized photochemical reduction and oxidation, J. Phys. Chem., 70 (1966) 3033–3036.
[39] S. Akir, A. Barras, Y. Coffinier, M. Bououdina, R. Boukherroub, A.D. Omrani, Eco-friendly synthesis of ZnO nanoparticles with different morphologies and their visible light photocatalytic performance for the degradation of Rhodamine B, Ceram. Int., 42 (2016) 10259–10265.
[40] T. Tharsika, A.S.M.A. Haseeb, S.A. Akbar, M. Thanihaichelvan, Tailoring ZnO nanostructures by spray pyrolysis and thermal annealing, Ceram. Int., 41 (2015) 5205–5211.
[41] O. Carp, A. Tirsoaga, R. Ene, A. Ianculescu, R.F. Negrea, P. Chesler, G. Ionita, R. Birjega, Facile, high yield ultrasound mediated protocol for ZnO hierarchical structures synthesis: Formation mechanism, optical and photocatalytic properties, Ultrason. Sonochem., 36 (2017) 326–335.
[42] F. Solis-Pomar, A. Jaramillo, J. Lopez-Villareal, C. Medina, D. Rojas, A.C. Mera, M.F. Meléndrez, E. Pérez-Tijerina, Rapid synthesis and photocatalytic activity of ZnO nanowires obtained through microwave-assisted thermal decomposition, Ceram. Int., 42 (2016) 18045–18052.
[43] L. Duan, X. Zhao, Z. Zheng, Y. Wang, W. Geng, F. Zhang, Structural, optical and photocatalytic properties of (Mg,Al)-co-doped ZnO powders prepared by sol–gelmethod, J. Phys. Chem. Solids., 76 (2015) 88–93.
[44] X. Xing, D. Deng, Y. Li, N. Chen, X. Liu, Y. Wang, Macro-/nanoporous Al-doped ZnO via self-sustained decomposition of metal-organic complexes for application in degradation of Congo red, Ceram. Int., 42 (2016) 18914–18924.
[45] X. Zhang, Y. Chen, S. Zhang, C. Qiu, High photocatalytic performance of high concentration Al-doped ZnO nanoparticles, Sep. Purif. Technol., 172 (2017) 236–241.
[46] B. Czech, M. Hojamberdiev, UVA- and visible-light-driven photocatalytic activity of three-layer perovskite Dion-Jacobson phase $CsBa_2M_3O_{10}$ (M = Ta, Nb) and oxynitride crystals in the removal of caffeine from model wastewater, J. Photochem. Photobiol., A., 324 (2016) 70–80.
[47] X. Yuan, Q. Jing, J. Chen, L. Li, Photocatalytic Cr(VI) reduction by mixed metal oxide derived from ZnAl layered double hydroxide, Appl. Clay Sci., 143 (2017) 168–174.
[48] G.P. Sahoo, S. Samanta, D.K. Bhui, S. Pyne, A. Maity, A. Misra, Hydrothermal synthesis of hexagonal ZnO microstructures in HPMC polymer matrix and their catalytic activities, J. Mol. Liq., 212 (2015) 665–670.
[49] F.M. Stringhini, E.L. Foletto, D. Sallet, D.A. Bertuol, O. Chiavone-Filho, C.A. Oller do Nascimento, Synthesis of porous zinc aluminate spinel ($ZnAl_2O_4$) by metal-chitosan complexation method, J. Alloys Compd., 588 (2014) 305–309.
[50] H.R. Liu, Y.J. Wei, Y.C. Hu, W. Jia, H. Ma, H.S. Jia, Effects of Ag nanoparticles on morphology and photocatalytic activities of GaN microrods arrays, Mater. Lett., 134 (2014) 119–122.
[51] A.A.A. Ahmed, A.T. Zainal, Z.H. Mohd, Z. Azmi, Improvement of the crystallinity and photocatalytic property of zinc oxide as calcination product of Zn–Al layered double hydroxide, J. Alloys Compd., 539 (2012) 154–160.
[52] S. Li, Z. Bai, D. Zhao, Characterization and friction performance of Zn/Mg/Al-CO_3 layered double hydroxides, Appl. Surf. Sci., 284 (2013) 7–12.
[53] Y. Guo, Z. Zhu, Y. Qiu, J. Zha, Adsorption of arsenate on Cu/Mg/Fe/La layered double hydroxide from aqueous solutions, J. Hazard. Mater., 239–240 (2012) 279–288.
[54] L. Zhang, C. Dai, X. Zhang, Y. Liu, J. Yan, Synthesis and highly efficient photocatalytic activity of mixed oxides derived from ZnNiAl layered double hydroxides, Trans. Nonferrous Met. Soc. China., 26 (2016) 2380–2389.
[55] Y. Yang, H. Li, F. Hou, J. Hu, X. Zhang, Y. Wang, Facile synthesis of ZnO/Ag nanocomposites with enhanced photocatalytic properties under visible light, Mater. Lett., 180 (2016) 97–100.
[56] S. Qourzal, N. Barka, M. Tamimi, A. Assabbane, A. Nounah, A. Ihlal, Y. Ait-Ichou, Sol–gel synthesis of TiO_2–SiO_2 photocatalyst for β-naphtholphotodegradation, Mater. Sci. Eng., C. 29 (2009) 1616–1620.
[57] I.K. Konstantinou, T.A. Albanis, TiO_2-assisted photocatalytic degradation of azo dyes in aqueous solution: kinetic and mechanistic investigations: a review, Appl. Catal. B Environ., 49 (2004) 1–14.
[58] N. Daneshvar, D. Salari, A.R. Khataee, Photocatalytic degradation of azo dye acid red 14 in water on ZnO as an alternative catalyst to TiO_2, J. Photochem. Photobiol. A Chem., 162 (2004) 317–322.
[59] A.A. Khodja, T. Sehili, J.F. Pilichowski, P. Boule, Photocatalytic degradation of 2-phenylphenol on TiO_2 and ZnO in aqueous suspensions, J. Photochem. Photobiol. A Chem., 141 (2001) 231–239.
[60] N. Barka, S. Qourzal, A. Assabbane, A. Nounah, Y. Ait-Ichou, Photocatalytic degradation of an azo reactive dye, Reactive Yellow 84, in water using an industrial titanium dioxide coated media, Arab. J. Chem., 3 (2010) 279–283.
[61] J. Fang, H. Fan, Y. Ma, Z. Wang, Q. Chang, Surface defects control for ZnO nanorods synthesized by quenching and their anti-recombination in photocatalysis, Appl. Surf. Sci., 332 (2015) 47–54.